IOP Publishing New J. Phys. 26 (2024) 073029 https://doi.org/10.1088/1367-2630/ad4737

New Journal of Physics
The open access journal at the forefront of physics

Deutsche Physikalische Gesellschaft DPG
IOP Institute of Physics

Published in partnership with: Deutsche Physikalische Gesellschaft and the Institute of Physics

OPEN ACCESS

RECEIVED
13 February 2024

ACCEPTED FOR PUBLICATION
3 May 2024

PUBLISHED
19 July 2024

PAPER

Majorana subsystem qubit codes that also correct odd-weight errors

Sourav Kundu* and **Ben Reichardt**

Ming Hsieh Department of Electrical Engineering, University of Southern California, Los Angeles, CA, United States of America
* Author to whom any correspondence should be addressed.

E-mail: souravku@usc.edu

Keywords: Majorana zero mode, fermionic errors, stabilizer codes, subsystem codes, quantum error correction, quantum fault-tolerance

Abstract

A potential platform for topological quantum computation is the Majorana-based tetron architecture. Its building blocks are superconducting islands called tetrons, which host four Majorana zero modes. Existing error correcting codes can correct even-weight errors on tetrons. In a previous proposal by us, we had shown that incorporating tetrons in the stabilizer group allows us to correct a combination of odd-weight errors and even-weight errors on tetrons. In this work, we show that inclusion of tetrons in the gauge group lets us create subsystem codes from conventional Pauli stabilizer codes, which can correct both kinds of errors. Compared to the previous approach, the current approach lets us construct codes with fewer stabilizer generators. This leads to shorter fault-tolerant sequence length, and improves the fault-tolerant pseudothreshold by as much as 84%.

1. Introduction

Topological quantum computation might be an important ingredient for quantum fault-tolerance [1–14]. In particular, the tetron architecture holds the promise of measurement-based quantum computation, without requiring anyon braiding [15–19].

We propose error correcting codes for this architecture, which can correct both even-weight errors as well as odd-weight errors on tetrons. The basic unit for this architecture is a tetron, which is a superconducting island that hosts four Majorana zero modes (MZMs). Figure 1(a) shows a schematic diagram for a tetron island that hosts the MZMs $\gamma_a, \gamma_b, \gamma_c, \gamma_d$ in locations a, b, c, d respectively. A group of tetrons can store quantum information in the form of operator parity. We can measure the parity of any Majorana operator that is supported on 0 or 2 MZMs per tetron. Such operators are used to define stabilizers and logical operators of Majorana codes. Figure 1(b) shows all 6 measurable operators in a tetron.

A tetron can be affected with errors on some of its MZMs. A 'bosonic error' affects two MZMs on some tetrons, and it can be corrected by a 'bosonic code' or a conventional Pauli stabilizer code. In a bosonic code, the Pauli operators X, Y, Z can be mapped to the Majorana operators $\gamma_b\gamma_c, \gamma_a\gamma_c, \gamma_a\gamma_b$, as shown in figure 1(b). However, such codes cannot correct 'fermionic errors' or odd-weight errors [20].

A tetron utilizes high charging energy to mitigate fermionic errors. Nonetheless, if a fermionic error persists for a significant duration, it has the potential to interfere with measurement outcomes and may extend to neighboring tetrons via connected measurements. Hence Knapp *et al* [18] suggests that it might be helpful to use 'fermionic codes' for correction of fermionic errors before they can spread.

In a previous work [21], we have proposed Majorana codes that can correct fermionic errors by incorporating each tetron in the stabilizer group. In this work, we show that we can construct subsystem codes capable of 'fermionic error correction' by using a classical code over the tetrons such that tetrons belong to the gauge group. The proposed subsystem codes require less stabilizer generators compared to the previous approach [21], and can potentially lead to smaller fault-tolerant sequences yielding higher

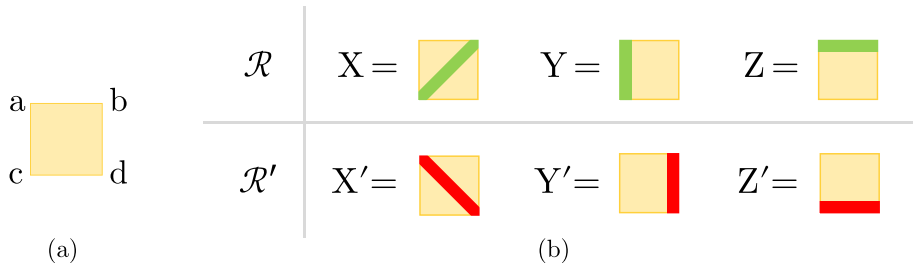

Figure 1. (a) A tetron has four Majorana zero modes at the four corners a,b,c,d. (b) There are six weight-2 Majorana operators in a tetron. (Reproduced from [21])

Table 1. This table compares the code capacity and fault-tolerant pseudothreshold between non-subsystem fermionic codes and currently proposed subsystem fermionic codes. The codes are compared at various values of noise bias η, which is the ratio between fermionic error probability and bosonic error probability. We observe that the $[\![10,1,2,d_f=3]\!]$ code has the shortest syndrome-measurement sequence that is fault-tolerant against a single error, and thus has the best fault-tolerant pseudothreshold among these codes. We observe that the threshold of subsystem codes exceed their non-subsystem counterparts. For the above codes and bias values, the threshold improvement percentage ranges from 10% to as much as 84%. The fault-tolerant sequences for these codes are provided in appendix A.

	Code capacity				Fault-tolerance pseudothreshold		
Code parameter	$\eta=0.1$	$\eta=1$	$\eta=10$	Fault-tolerant length	$\eta=0.1$	$\eta=1$	$\eta=10$
$[\![10,1,d_f=6]\!]$	0.137	0.196	0.423	9	0.001 34	0.001 45	0.001 46
$[\![10,1,2,d_f=3]\!]$	0.135	0.169	0.255	8	0.001 64	0.001 70	0.001 61
$[\![12,1,d_f=6]\!]$	0.103	0.177	0.391	14	0.000 43	0.000 45	0.000 45
$[\![12,1,1,d_f=6]\!]$	0.103	0.176	0.346	12	0.000 60	0.000 62	0.000 62
$[\![12,1,3,d_f=3]\!]$	0.097	0.122	0.197	12	0.000 59	0.000 60	0.000 59
$[\![14,1,d_f=6]\!]$	0.072	0.128	0.418	16	0.000 27	0.000 28	0.000 29
$[\![14,1,4,d_f=3]\!]$	0.067	0.077	0.155	12	0.000 47	0.000 51	0.000 51

pseudothreshold. This is depicted in table 1, which compares codes constructed using the previous approach, with currently proposed codes.

In section 2, we provide a brief overview of Majorana operators and how they can be affected by errors. We discuss some experimental challenges that hindered previous attempts of fermionic error correction. Fortunately, our proposal does not require any experimental changes, and we distinguish fermionic errors from bosonic errors by using two sets of operators shown in figure 1(b).

In section 3, we describe a general recipe of fermionic subsystem code construction using Pauli stabilizer codes and classical codes. We choose a Pauli stabilizer code with parameters $[\![n,k_1,d_b]\!]$, and introduce additional stabilizers supported on one or more tetrons in accordance with an $[n,k_2,d_c]$ classical code. This results in a $[\![2n,k_1,d_f]\!]$ subsystem code with k_2 gauge qubits, where the fermionic code distance d_f is bounded by $d_b \leqslant d_f \leqslant 2d_b$. For convenience, we will denote this subsystem code as $[\![2n,k_1,k_2,d_f]\!]$, and will continue to use this four-parameter notation later. We provide error analysis on some small codes constructed with this recipe, as well as examples of some fault-tolerant schemes.

2. Background

The basic unit of this architecture is a superconducting island that hosts an even number of MZMs. Islands with four MZMs are called tetrons, islands with six MZMs are called hexons, islands with eight MZMs are called octons, and so on. We shall focus on the tetron architecture and propose error correction schemes for it.

2.1. Majorana operators

We begin with a brief overview of the mathematical properties of Majorana operators. We consider a system with an even number of MZMs, which are denoted as $\gamma_1,\gamma_2,\ldots\gamma_{N_{\text{Maj}}}$. They satisfy these three properties:

$$\gamma_j=\gamma_j^\dagger,\ \gamma_j^2=\mathbb{I},\ \{\gamma_j,\gamma_k\}=2\delta_{j,k}.$$

A Majorana operator supported on the MZM set $S\subseteq\{1,2,\ldots,N_{\text{Maj}}\}$ can be defined as $|S\rangle=\sum_{j\in S}|j\rangle$, where the MZM $|j\rangle$ is a basis vector in $\mathbb{F}_2^{N_{\text{Maj}}}$. The commutation relations for two arbitrary Majorana operators$|A\rangle$ and $|B\rangle$ is given by $|A\rangle\times|B\rangle=(-1)^{|A|\cdot|B|+|A\cap B|}\times|B\rangle\times|A\rangle$. However, in practice, we can only

measure the parity of Majorana operators that are supported on even number of MZMs per island. The commutation relations are simpler for them. Two operators with even weight commute if they have even overlap, and anticommute otherwise. We can use this to verify the commutation relations for the Pauli operators shown in figure 1(b).

The parity of a Majorana operator can be affected by errors. If errors affect an odd number of MZMs in the operator support, that toggles its parity. However, if a Majorana operator is affected by even number of errors, its parity remains unchanged.

2.2. Challenges of fermionic error correction

Fermionic error correction can help to correct fermionic errors before they spread via connected measurements. Although some of the previously proposed codes are theoretically capable of fermionic error correction [22, 23], there are experimental challenges for their implementation. We discuss some general challenges that hindered development of fermionic codes.

Firstly, it is experimentally challenging to perform a four-MZM parity measurement on a tetron [18]. Otherwise it would have been trivial to identify tetrons that have odd-weight errors.

Secondly, it is difficult to dynamically adjust the number of MZMs on an island, because it requires careful tuning of experimental parameters [18].

Another approach was suggested by Bomantara and Gong [24] for correction of a weight-1 error on a nanowire. They suggested tuning the system parameters to generate additional MZMs at ends of the nanowire. A stabilizer code can be defined over the two original MZMs and the additional generated MZMs, which can correct a weight-1 error on the nanowire. This is experimentally challenging as well.

Fortunately, our fermionic error correction proposal does not require any experimental changes and can be achieved by conventional measurements that span two MZMs per tetron.

2.3. Principle of fermionic error correction

A tetron island hosts four MZMs, and is maintained in even parity state by high charging energy. As the tetron has overall even parity, so if we conceptually divide the tetron in two halves, then both halves must have the same parity. Now consider the 6 operators shown in figure 1(b), which are grouped in two sets:

$$\begin{aligned} \mathcal{R} &= \{X, Y, Z\}, \qquad \text{where } X = \gamma_b\gamma_c,\ Y = \gamma_a\gamma_c,\ Z = \gamma_a\gamma_b \\ \mathcal{R}' &= \{X', Y', Z'\}, \quad \text{where } X' = \gamma_a\gamma_d, Y' = \gamma_d\gamma_b, Z' = \gamma_c\gamma_d. \end{aligned}$$

Note that parity measurement would give the same result for two corresponding operators in $\mathcal{R}$ and $\mathcal{R}'$. For example, parity measurement would give the same result for operators X and X', the same result for operators Y and Y', and the same result for operators Z and Z'. This remains true even if the tetron is affected by an even-weight error.

However, things change when the charging energy protection is insufficient to maintain even parity state of the tetron. If an odd-weight error occurs on a tetron, then parity measurement would give opposite results for operators X and X', opposite results for operators Y and Y', and opposite results for operators Z and Z'.

Thus, whether two corresponding operators from $\mathcal{R}$ and $\mathcal{R}'$ have the same parity or the opposite parity can be used as a test to identify whether an error has even weight or odd weight. We can use this idea to develop codes which correct odd-weight errors.

3. BC $\mapsto$ FS: Fermionic subsystem codes from bosonic and classical codes

We show that a non-subsystem bosonic code on n qubits and a classical code over n bits can be used to construct a subsystem fermionic code over n tetrons. We apply this recipe to obtain several small subsystem fermionic codes.

3.1. Notations for Majorana codes

Let us define some common notations that we will use for Majorana stabilizer codes and bosonic stabilizer codes.

A Pauli code with parameters $[\![n, k, d_b]\!]$ represents a code over n physical qubits with k logical qubits, where the logical operators have a least Pauli weight of d_b.

A Majorana code with parameters $[\![2n, k_1, k_2, d_f]\!]$ represents a code over n tetrons with k_1 logical qubits and k_2 gauge qubits, where the dressed logical operators have a least Majorana weight of d_f. If a Majorana code has no gauge qubits, then it is simply denoted by three parameters—$[\![2n, k_1, d_f]\!]$.

If an $[\![n, k, d_b]\!]$ Pauli code is converted to a Majorana code by using the Pauli definitions given in figure 1(b), then it would have parameters $[\![2n, k, d_f]\!]$, where $d_f = 2d_b$. Out of $2n$ degrees of freedom that n

tetrons can have, $n-k$ degrees are restricted by stabilizer measurements. Furthermore, if we assume that each tetron is constrained to even parity by means of high charging energy, then it restricts another n degrees of freedom. Thus, we are left with k logical qubits for the k degrees of freedom left in the code. The logical operators of the Majorana code would have a least Majorana weight $d_f = 2d_b$, since each Pauli operator corresponds to two MZMs. The code distance subscript b indicates that this is the bosonic distance corresponding to the least Pauli weight of the logical operators. The code distance subscript f indicates that this is the fermionic distance corresponding to the least Majorana weight of the dressed logical operators, which is also equal to the smallest error weight that can affect a logical qubit without producing any syndrome.

Now for fermionic error correction, we cannot assume that n degrees of freedom are restricted by high charging energy. Instead, we would need to manually restrict these degrees of freedom by introducing additional stabilizer measurements, as we will see in the subsequent sections.

3.2. Recipe for fermionic code construction

We use an $[\![n, k_b, d_b]\!]$ non-subsystem bosonic code and an $[n, k, d_c]$ classical code to derive a $[\![2n, k_b, k, d_f]\!]$ subsystem fermionic code.

We start with the stabilizers and logical operators of the $[\![n, k_b, d_b]\!]$ code and convert their Pauli operators X, Y, Z to the Majorana operators $X = \gamma_b\gamma_c, Y = \gamma_a\gamma_c, Z = \gamma_a\gamma_b$, according to figure 1(b). For example, we can choose a $[\![5, 1, 3]\!]$ Pauli stabilizer code with stabilizer generators *IZXZX*, *XXIZZ*, *ZIXXZ*, and *XZZXI*. These generators are illustrated in row A of figure 2(a). The corresponding logical operators are illustrated in the first row of figure 2(b).

Then we choose the classical code $[n, k, d_c]$ with parity matrix H and generator matrix G. We choose G to be in the systematic form $[I_k|P]$ where I_k is a $k \times k$ identity matrix and P is a $k \times (n-k)$ matrix. Then we add tetron stabilizers according to the rows of its parity matrix.

For example, we can choose the $[5, 2, 3]$ classical code with parity matrix

$$H = \begin{bmatrix} 1 & 1 & 0 & 0 & 1 \\ 0 & 1 & 1 & 0 & 1 \\ 0 & 0 & 0 & 1 & 1 \end{bmatrix}$$

and a systematic generator matrix

$$G = \begin{bmatrix} 1 & 0 & 1 & 1 & 1 \\ 0 & 1 & 0 & 1 & 1 \end{bmatrix}.$$

Since the first row of H is 11001, then we need to add the stabilizer $T_1T_2T_5$ comprising the first, second and fifth tetrons. Now, we cannot directly measure the parity of one or more tetrons. So in order to add such a stabilizer, we would choose an existing stabilizer, for example $S_1 = XXIZZ$, that is supported on at least the first, second and fifth tetrons. Then we add a modified stabilizer where the operators on the first, second and fifth tetrons are switched from $\mathcal{R}$ to $\mathcal{R}'$, for example $S_{1m} = X'X'IZZ'$. This ensures that $S_1 \times S_{1m} = T_1T_2T_5$ belongs to the stabilizer group.

In this step, it is essential that the stabilizer code and the classical code are compatible with each other, such that there exists a stabilizer supported on the non-zero tetrons in each row of the parity matrix.

The resulting subsystem fermionic code has $n - k_b$ stabilizers from the bosonic code and $n - k$ stabilizers from the classical code. This code has the same k_b logical qubits as the bosonic code.

This code also has k gauge qubits, corresponding to the k rows of the generator matrix of the classical code. Each row of the generator matrix can be mapped to two gauge operators, the first being a tetron operator at the first non-zero entry of the generator matrix row. The second operator is a fermionic operator corresponding to γ_d on all non-zero entries of that generator matrix row. For example, if the generator matrix row is 11001, then the gauge operators are T_1 (the first tetron) and $\gamma_{d1}\gamma_{d2}\gamma_{d5}$ (supported on γ_d operator of tetrons 1, 2, and 5). This provides us with $2k$ gauge operators which generate a group of 2^{2k} size, and contains k gauge qubits.

Claim. The above code construction utilizing an $[\![n, k_b, d_b]\!]$ non-subsystem bosonic code and an $[n, k, d_c]$ classical code results in a subsystem code with k gauge qubits.

Proof. We will show that the chosen gauge operators form generators of a gauge group.

- Suppose the classical code has parity matrix H and generator matrix G. If the group formed by rows of H contain any single tetron at index D, then the entire column D of the generator matrix must be zero so that G remains orthogonal with H. As we have chosen our tetron gauges from non-zero locations of the generator matrix rows, so these chosen tetrons do not belong to the stabilizer group.

- As the logical operators are only supported on $\gamma_a, \gamma_b, \gamma_c$ but not the γ_d operators, so the tetrons cannot belong to the group of logical operators.
- The k chosen fermionic operators do not belong to stabilizer group or logical operator group. As the stabilizers and logical operators are supported on two MZMs per tetrons, so their group cannot have any fermionic operator.
- The k chosen tetrons are independent of each other as they have no overlap.
- The k chosen fermionic operators are independent of each other because the rows of generator matrix are independent of each other.
- The tetrons and fermionic operators are independent of each other since the fermionic operators are supported only on γ_d operators and none of $\gamma_a, \gamma_b, \gamma_c$ operators.
- The k chosen fermionic operators commute with all the tetron stabilizers formed by the rows of parity matrix H, since G and H are orthogonal.
- The k chosen fermionic operators are entirely supported on γ_d operators, whereas the original Pauli stabilizers of the bosonic code as well as the logical operators are supported only on $\gamma_a, \gamma_b, \gamma_c$ operators. So the k chosen fermionic operators have no intersection with them, and so commute with them.
- The tetrons commute with all stabilizers and logical operators.

Thus we have k tetrons and k fermionic operators which are independent of each other, as well as independent of stabilizers and logical operators. They commute with both stabilizers and logical operators, and hence these $2k$ operators form a gauge group of size 2^{2k}, which can accommodate k gauge qubits. □

Note that the least weight of all fermionic gauges, or the least weight of the group formed by generator matrix rows is the same as the classical code distance d_c.

3.3. Code distance

Code distance of subsystem codes are given by the least weight of all nontrivial dressed logical operators. If a logical operator of minimum weight $2d_b$ and a fermionic gauge operator are supported on the same tetrons, then the dressed logical operator formed by their product has the least Majorana weight d_b. If their support is different, then the dressed logical operator would have a higher weight. Thus, the code distance d_f of the subsystem code is bounded by $d_b \leqslant d_f \leqslant 2d_b$. The code distance for the proposed codes are evaluated by exhaustive search.

3.4. Decoder

We use the BPOSD decoder, proposed by Roffe *et al* [25, 26] for correcting errors in the subsequent examples. We use the 'product_sum' method for belief propagation, the 'osd_cs' method for the ordered statistics decoder, a a maximum of five iterations, and a search depth of $2N+1$ where N is the number of tetrons.

3.5. Example 1: $[\![10, 1, 2, d_f = 3]\!]$ subsystem code

We derive the $[\![10, 1, 2, d_f = 3]\!]$ subsystem Majorana fermionic code from the $[\![5, 1, 3]\!]$ Pauli stabilizer code and the $[5, 2, 3]$ classical code. The stabilizer generators of this code are shown in rows A and B of figure 2(a), and its logical and gauge qubits are illustrated in figure 2(b). The third row of figure 2(a) shows that the product of corresponding stabilizer generators in rows A and B yields tetron sets in the stabilizer group. These tetron stabilizers correspond to the rows of a parity matrix H shown in figure 2(c). The two gauge qubits correspond to the two rows of the generator matrix G shown in figure 2(c). These two matrices characterize the $[5, 2, 3]$ classical code. The smallest error which affects the logical qubit but yields zero syndrome is $\gamma_{b3}\gamma_{c4}\gamma_{b5}$, so the Majorana code has distance $d_f = 3$. As each stabilizer generator overlaps with another generator, so we require seven time steps for syndrome measurement.

Figure 2 illustrates that the rows of the parity matrix correspond to the tetron stabilizers, and the rows of the generator matrix correspond to the gauge operators. Note that for each gauge qubit, one gauge operator corresponds to a tetron on the first non-zero entry of the generator matrix row, and another gauge operator is a fermionic operator corresponding to γ_d on all non-zero entries of that generator matrix row. For example, if the generator matrix row is 11001, then the gauge operators are T_1 (the first tetron) and $\gamma_{d1}\gamma_{d2}\gamma_{d5}$ (supported on γ_d operator of tetrons 1, 2, and 5). We can verify the commutation relation between these operators by inspection.

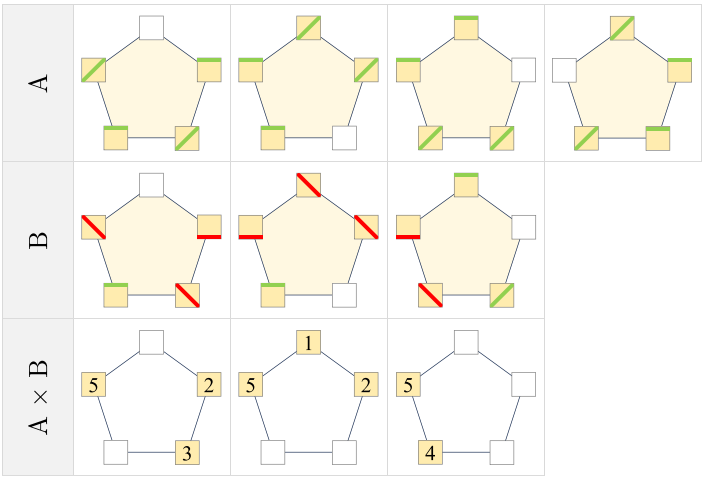

(a)

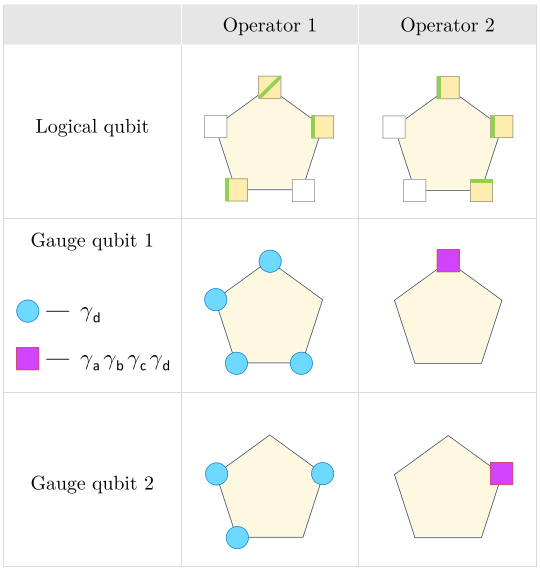

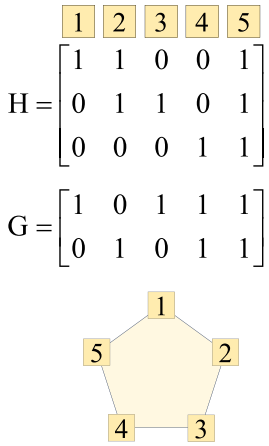

(b) (c)

Figure 2. (a) This figure shows the 7 stabilizer generators of the $[\![10, 1, 2, d_f = 3]\!]$ Majorana fermionic subsystem code in the rows A and B. The third row shows the stabilizer formed by the corresponding generators in the first and the second rows. Each stabilizer in the third row is a set of tetrons, corresponding to the rows of parity matrix H. (b) This figure shows the logical qubit and the gauge qubits of the $[\![10, 1, 2, d_f = 3]\!]$ Majorana fermionic subsystem code. Each gauge qubit corresponds to a row of the generator matrix G. (c) This figure shows the classical parity matrix H and the generator matrix G of the $[5, 2, 3]$ classical code. The tetron numbering scheme shown in this figure is used for the matrix columns.

3.6. Example 2: $[\![12, 1, 3, d_f = 3]\!]$ subsystem code

We derive the $[\![12, 1, 3, d_f = 3]\!]$ subsystem Majorana fermionic code from the $[\![6, 1, 3]\!]$ Pauli stabilizer code and the $[6, 3, 3]$ classical code. The stabilizer generators of this code are shown in rows A and B of figure 3(a), and its logical and gauge qubits are illustrated in figure 3(b). The third row of figure 3(a) shows that the product of corresponding stabilizer generators in rows A and B yields tetron sets in the stabilizer group. These tetron stabilizers correspond to the rows of a parity matrix H shown in figure 3(c). The three gauge qubits correspond to the three rows of the generator matrix G shown in figure 3(c). These two matrices characterize the $[6, 3, 3]$ classical code. The smallest error which affects the logical qubit but yields zero syndrome is $\gamma_{c2}\gamma_{c3}\gamma_{c6}$, so the Majorana code has distance $d_f = 3$. This code has eight stabilizer generators, but two of them can be parallelly measured, so we need seven time steps for syndrome measurement.

Figure 3 illustrates that the rows of the parity matrix correspond to the tetron stabilizers, and the rows of the generator matrix correspond to the gauge operators.

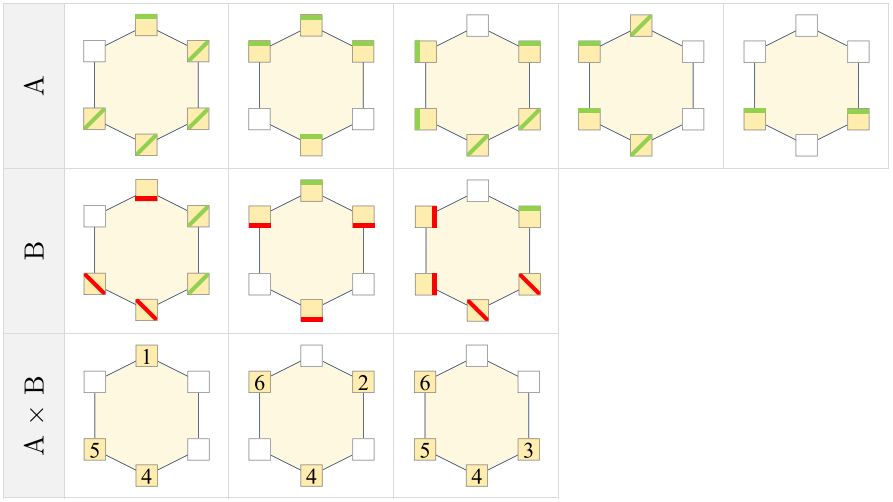

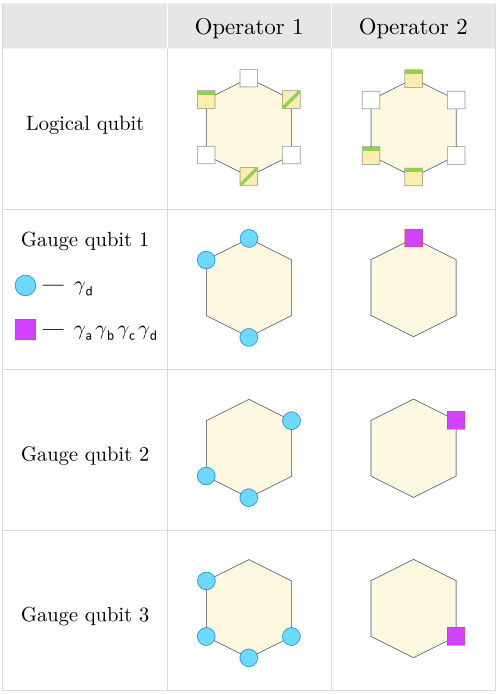

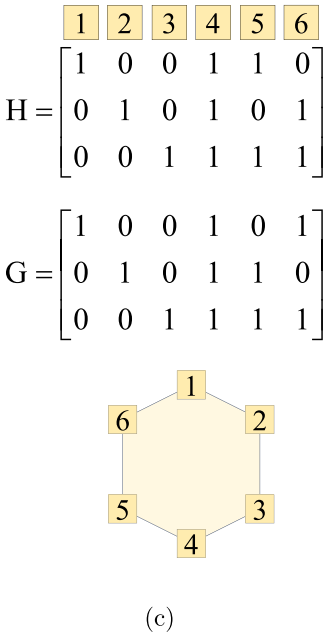

Figure 3. (a) This figure shows the 8 stabilizer generators of the $[\![12, 1, 3, d_f = 3]\!]$ Majorana fermionic subsystem code in the rows *A* and *B*. The third row shows the stabilizer formed by the corresponding generators in the first and the second rows. Each stabilizer in the third row is a set of tetrons, corresponding to the rows of parity matrix *H*. (b) This figure shows the logical qubit and the gauge qubits of the $[\![12, 1, 3, d_f = 3]\!]$ Majorana fermionic subsystem code. Each gauge qubit corresponds to a row of the generator matrix *G*. (c) This figure shows the classical parity matrix *H* and the generator matrix *G* of the $[6, 3, 3]$ classical code. The tetron numbering scheme shown in this figure is used for the matrix columns.

3.7. Example 3: $[\![14, 1, 4, d_f = 3]\!]$ subsystem code

We derive the $[\![14, 1, 4, d_f = 3]\!]$ subsystem Majorana fermionic code from the $[\![7, 1, 3]\!]$ Pauli Steane code and the $[7, 4, 3]$ classical Hamming code. The stabilizer generators of this code are shown in rows *A* and *B* of figure 4(a), and its logical and gauge qubits are illustrated in figure 4(b). The third row of figure 4(a) shows that the product of corresponding stabilizer generators in rows *A* and *B* yields tetron sets in the stabilizer group. These tetron stabilizers correspond to the rows of a parity matrix *H* shown in figure 4(c). The four gauge qubits correspond to the four rows of the generator matrix *G* shown in figure 4(c). These two matrices characterize the $[7, 4, 3]$ classical Hamming code. The smallest error which affects the logical qubit but yields zero syndrome is $\gamma_{a1}\gamma_{a6}\gamma_{a7}$, so the Majorana code has distance $d_f = 3$. This code has nine stabilizer generators, all of which overlap with one another. Hence, we require nine time steps for syndrome measurement.

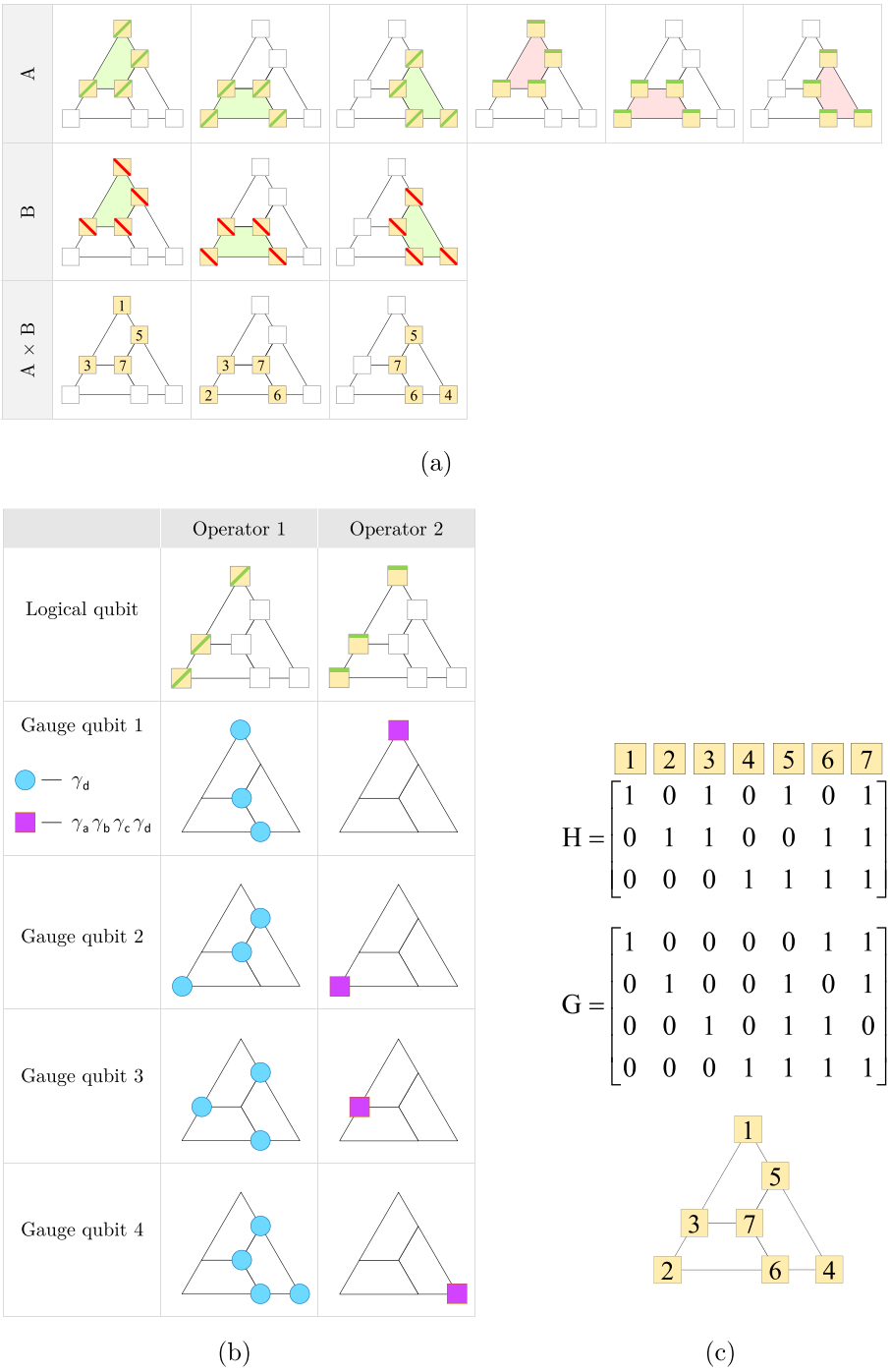

Figure 4. (a) This figure shows the 9 stabilizer generators of the $[\![14, 1, 4, d_f = 3]\!]$ Majorana fermionic subsystem code in the rows *A* and *B*. The third row shows the stabilizer formed by the corresponding generators in the first and the second rows. Each stabilizer in the third row is a set of tetrons, corresponding to the rows of parity matrix *H*. (b) This figure shows the logical qubit and the gauge qubits of the $[\![14, 1, 4, d_f = 3]\!]$ Majorana fermionic subsystem code. Each gauge qubit corresponds to a row of the generator matrix *G*. (c) This figure shows the classical parity matrix *H* and the generator matrix *G* of the $[7, 4, 3]$ classical code. The tetron numbering scheme shown in this figure is used for the matrix columns.

Figure 4 illustrates that the rows of the parity matrix correspond to the tetron stabilizers, and the rows of the generator matrix correspond to the gauge operators.

3.8. Code capacity

We analyze four fermionic subsystem codes, and plot their variation of pseudothreshold with noise bias in figure 5. Their logical error plots at various noise bias are provided in appendix B. The bosonic codes and classical codes from which these four fermionic subsystem codes are obtained are listed below:

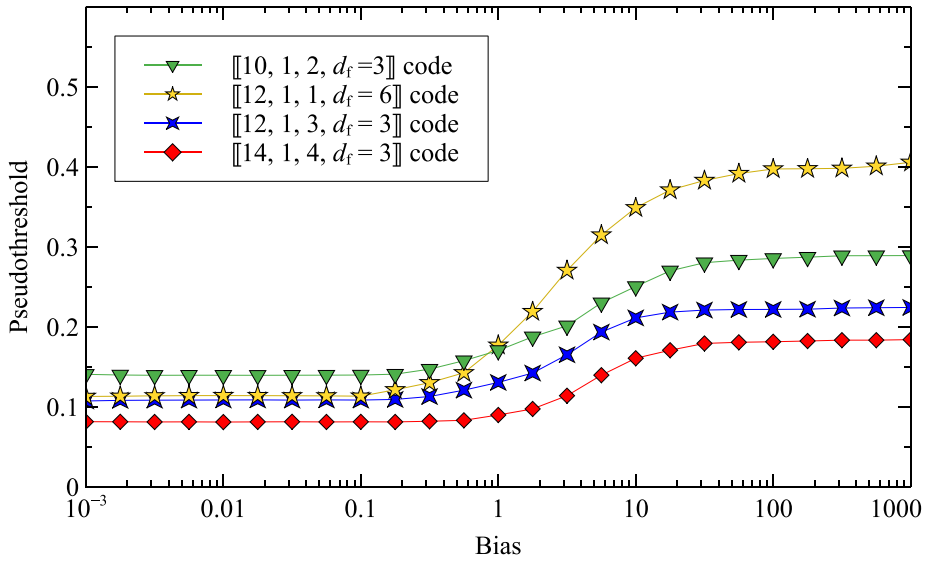

Figure 5. The figure shows the variation of pseudothreshold with noise bias for $[\![10,1,2,d_f=3]\!]$, $[\![12,1,1,d_f=6]\!]$, $[\![12,1,3,d_f=3]\!]$ and $[\![14,1,4,d_f=3]\!]$ subsystem codes.

- $[\![5,1,3]\!]+[5,2,3]\rightarrow[\![10,1,2,d_f=3]\!]$
- $[\![6,1,3]\!]+[6,1,6]\rightarrow[\![12,1,1,d_f=6]\!]$
- $[\![6,1,3]\!]+[6,3,3]\rightarrow[\![12,1,3,d_f=3]\!]$
- $[\![7,1,3]\!]+[7,4,3]\rightarrow[\![14,1,4,d_f=3]\!]$.

For the above Majorana fermionic subsystem codes, the stabilizers of the $[\![5,1,3]\!]$, $[\![6,1,3]\!]$, and $[\![7,1,3]\!]$ codes are illustrated in figures 2(a), 3(a), and 4(a) respectively. The classical codes $[5,2,3]$, $[6,3,3]$, $[7,4,3]$ are defined in figures 2(c), 3(c), and 4(c) respectively. The $[6,1,6]$ code is a classical repetition code.

In this analysis, we utilize a biased noise model. We consider that fermionic errors are η times more likely to occur than bosonic errors. There are three possible modes for bosonic errors—X, Y, Z errors, each of which occurs with equal probability $p_X=p_Y=p_Z=p/(3\eta+3)=p_b/3$. There are 4 possible modes for fermionic errors — $\gamma_a,\gamma_b,\gamma_c,\gamma_d$, each of which occurs with equal probability $p_{\gamma_a}=p_{\gamma_b}=p_{\gamma_c}=p_{\gamma_d}=p\eta/(4\eta+4)=p_f/4$. We use the BPOSD decoder to obtain the logical error rates for bias values $\eta=0.1,1,10$. We evaluate the pseudothreshold as the p value below which the logical error rate is lower than the physical error rate. Note that the physical error rate is given by $p_b+3p_f/4$ since a tetron qubit is affected by all bosonic errors but only 3 out of 4 fermionic errors.

3.9. Fault tolerance

Fault-tolerance can be achieved by careful ordering of stabilizers, and might require some redundant stabilizer measurements.

For example, figure 6 shows a fault-tolerant sequence for the $[\![10,1,2,d_f=3]\!]$ fermionic subsystem code, which utilizes only one additional redundant stabilizer measurement. This sequence can tolerate one bosonic or one fermionic error, either at the input or at any intermediate stage. We analyze this sequence for noise bias $=\eta$, bosonic error rate $p_b=p/(\eta+1)$, fermionic error rate $p_f=p\eta/(\eta+1)$, and measurement error rate p. The fault-tolerance threshold for this sequence is illustrated in figure 7 for bias values of 0.1, 1 and 10. The fault-tolerant sequences for other codes are provided in appendix A, and their fault-tolerance logical plots are provided in appendix B.

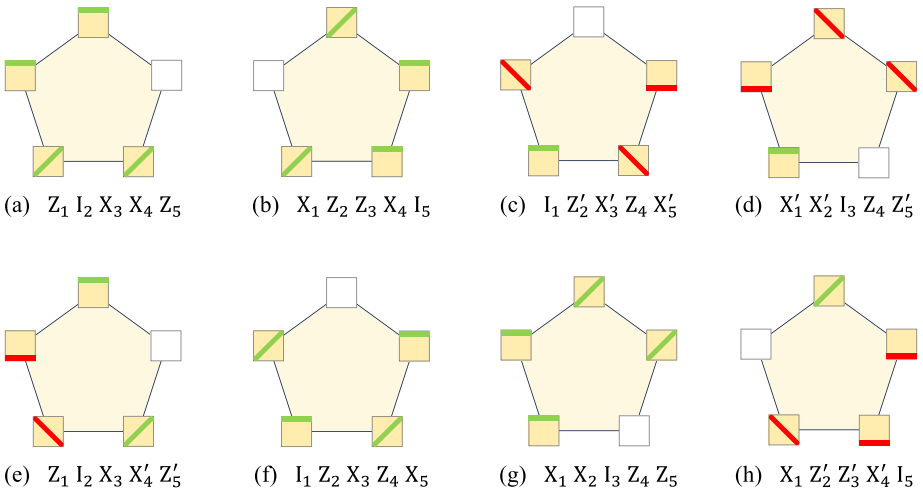

Figure 6. (a)–(h) demonstrate a sequence of fault-tolerant measurements for the $[\![10, 1, 2, d_f = 3]\!]$ fermionic subsystem code. This sequence can tolerate one bosonic error or one fermionic error. The tetron operators follow the same notations as figure 1(b).

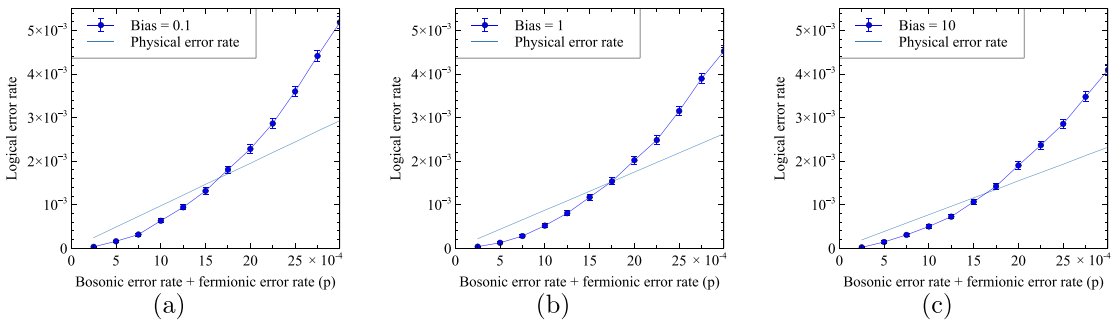

Figure 7. The logical error plots for the fault-tolerant implementation of the $[\![10, 1, 2, d_f = 3]\!]$ code are given in figures (a)–(c) for bias values $\eta = 0.1, 1, 10$ respectively. The graphs also show the 95% confidence intervals.

4. Conclusion

We have shown that subsystem fermionic codes can be constructed from Pauli stabilizer codes. We compare the currently proposed codes with previously proposed non-subsystem codes and find that the current proposal leads to shorter fault-tolerant sequences and higher fault-tolerant pseudothreshold.

Data availability statement

All data that support the findings of this study are included within the article (and any supplementary files).

Acknowledgments

This work is supported by MURI Grant FA9550-18-1-0161. This material is based on work supported by the U.S. Department of Energy, Office of Science, National Quantum Information Science Research Centers, Quantum Systems Accelerator.

Table A1. This lists the fault-tolerant sequence for the codes tabulated in table 1.

$[\![10,1,d_f=6]\!]$	$[\![10,1,2,d_f=3]\!]$	$[\![12,1,d_f=6]\!]$	$[\![12,1,1,d_f=6]\!]$	$[\![12,1,3,d_f=3]\!]$	$[\![14,1,d_f=6]\!]$	$[\![14,1,4,d_f=3]\!]$
$X_1'Z_2Z_3X_4$	$Z_1X_3X_4Z_5$	$Z_1X_2X_3X_4X_5$	$Z_1X_2X_3X_4X_5$	$Z_1X_2X_3X_4X_5$	$X_1X_2X_3X_4$	$X_1X_3X_5X_7$
$X_2'Z_3Z_4X_5$	$X_1Z_2Z_3X_4$	$Z_1Z_2Z_4Z_6$	$Z_1Z_2Z_4Z_6$	$Z_1Z_2Z_4Z_6$	$X_2X_4X_6X_7$	$X_2X_3X_6X_7$
$X_1X_3'Z_4Z_5$	$Z_2'X_3'Z_4X_5'$	$Z_2X_3X_4Y_5Y_6$	$Z_2X_3X_4Y_5Y_6$	$Z_2X_3X_4Y_5Y_6$	$X_3X_4X_5X_6$	$X_4X_5X_6X_7$
$Z_1X_2X_4'Z_5$	$X_1'X_2'Z_4Z_5'$	$X_1X_4Z_5Z_6$	$X_1X_4Z_5Z_6$	$X_1X_4Z_5Z_6$	$Z_1Z_2Z_3Z_4$	$Z_1Z_3Z_5Z_7$
$Z_1Z_2X_3X_5'$	$Z_1X_3X_4'Z_5'$	Z_3Z_5	Z_3Z_5	Z_3Z_5	$Z_2Z_4Z_6Z_7$	$Z_2Z_3Z_6Z_7$
$X_1Z_2Z_3X_4$	$Z_2X_3Z_4X_5$	$Z_1'X_2X_3X_4X_5$	$Z_1'X_2'X_3X_4X_5$	$Z_1'X_2X_3X_4'X_5'$	$Z_3Z_4Z_5Z_6$	$Z_4Z_5Z_6Z_7$
$X_2Z_3Z_4X_5$	$X_1X_2Z_4Z_5$	$Z_1Z_2'Z_4Z_6$	$Z_1Z_2Z_4Z_6'$	$Z_1Z_2'Z_4'Z_6'$	$X_1'X_2X_3X_4$	$X_1'X_3'X_5'X_7'$
$X_1X_3Z_4Z_5$	$X_1Z_2'Z_3'X_4'$	$Z_2X_3'X_4Y_5Y_6$	$Z_2X_3X_4Y_5'Y_6'$	$Z_2X_3'X_4'Y_5'Y_6'$	$X_3'X_4X_5X_6$	$X_2'X_3'X_6'X_7'$
$Z_1X_2X_4Z_5$		$X_1X_4'Z_5Z_6$	$X_1X_4'Z_5'Z_6$	$Z_1X_2X_3X_4X_5$	$X_2'X_4X_6X_7$	$X_4'X_5'X_6'X_7'$
		Z_3Z_5'	$Z_3'Z_5'$	$Z_1Z_2Z_4Z_6$	$Z_1Z_2Z_3Z_4'$	$Z_1'Z_3'Z_5'Z_7'$
		$Z_1Z_2Z_4Z_6'$	$Z_2X_3X_4Y_5Y_6$	$Z_1'X_2X_3X_4'X_5'$	$Z_3Z_4Z_5'Z_6$	$Z_2'Z_3'Z_6'Z_7'$
		$Z_1Z_2Z_4Z_6$	$Z_2X_3'X_4'Y_5Y_6$	$Z_2'X_3X_4'Y_5Y_6'$	$Z_2Z_4Z_6'Z_7$	$Z_4'Z_5'Z_6'Z_7'$
		$Z_1X_2X_3X_4'X_5$			$Z_2Z_4Z_6Z_7'$	
		$Z_2X_3X_4Y_5'Y_6$			$Y_1'Y_2'Y_3'Y_4'$	
					$Y_2'Y_4'Y_6'Y_7'$	
					$Y_3'Y_4'Y_5'Y_6'$	

Appendix A. Fault-tolerant sequence

The fault-tolerant sequences for the codes provided in table 1 are listed in table A1. These syndrome measurement sequence can tolerate 1 bosonic or 1 fermionic error, either at the input or at any intermediate stage. We can observe that the subsystem construction leads to smaller fault-tolerance sequences as compared to the non-subsystem construction.

Appendix B. Code capacity and fault-tolerance

The code capacity plots and fault-tolerance plots of select fermionic subsystem codes and non-subsystem codes are shown in figures B1 and B2 respectively. As code capacity does not consider intermediate errors, so they do not reflect the advantage of shorter syndrome measurement sequences in subsystem codes. In contrast, fault-tolerance plots show that subsystem codes have higher threshold as compared to their non-subsystem counterparts.

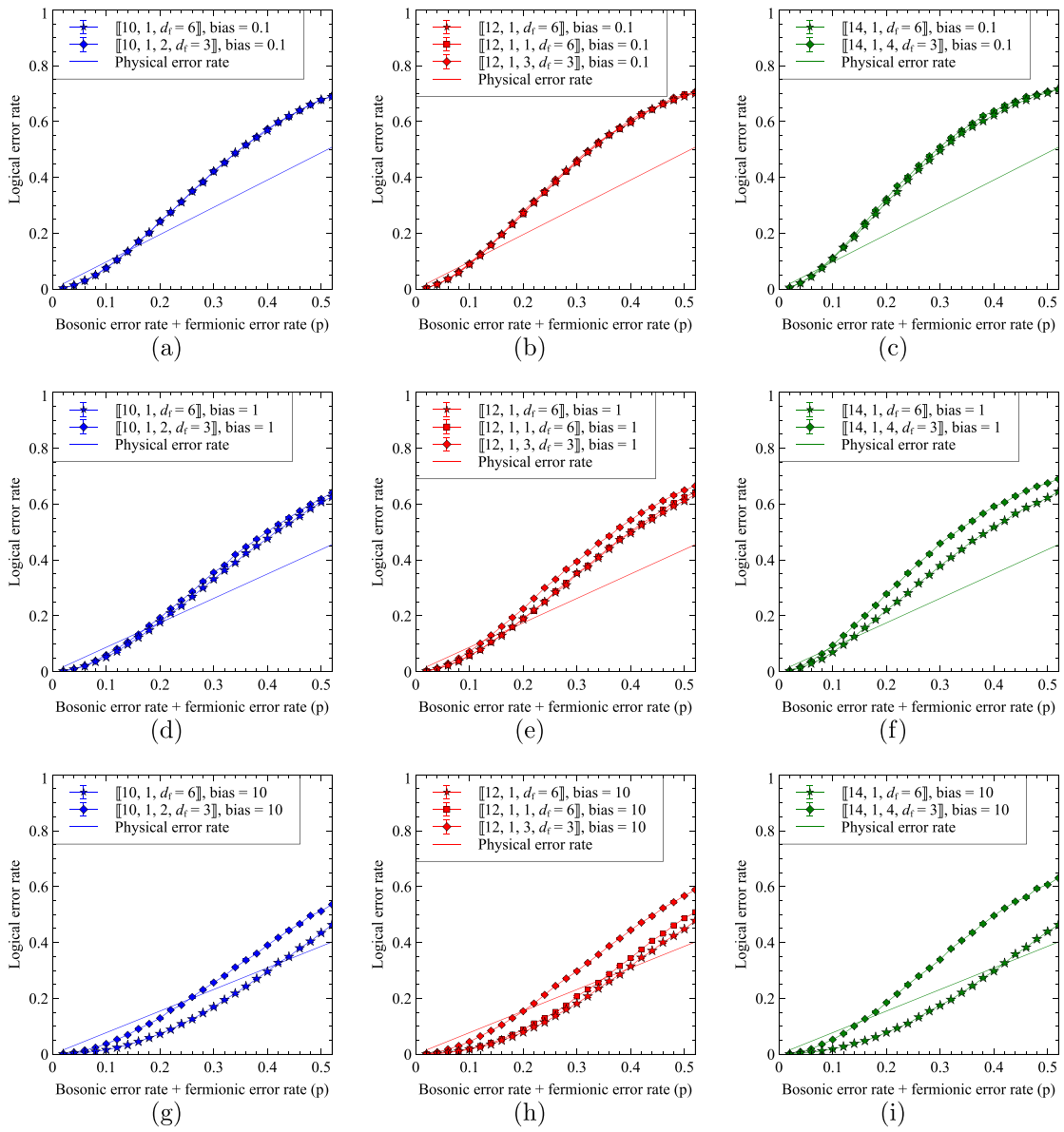

Figure B1. Code capacity logical error plots for currently proposed fermionic subsystem codes as well as previously proposed non-subsystem fermionic codes. The left column shows the plot for the five tetron codes, the middle column shows the plot for the six tetron codes, and the right column shows the plot for the seven tetron codes. In these plots, the 95% confidence interval bars are smaller than the marker size. (Top row) The three plots show the variation of logical error rate with p for bias $\eta = 0.1$. (Middle row) The three plots show the variation of logical error rate with p for bias $\eta = 1$. (Bottom row) The three plots show the variation of logical error rate with p for bias $\eta = 10$.

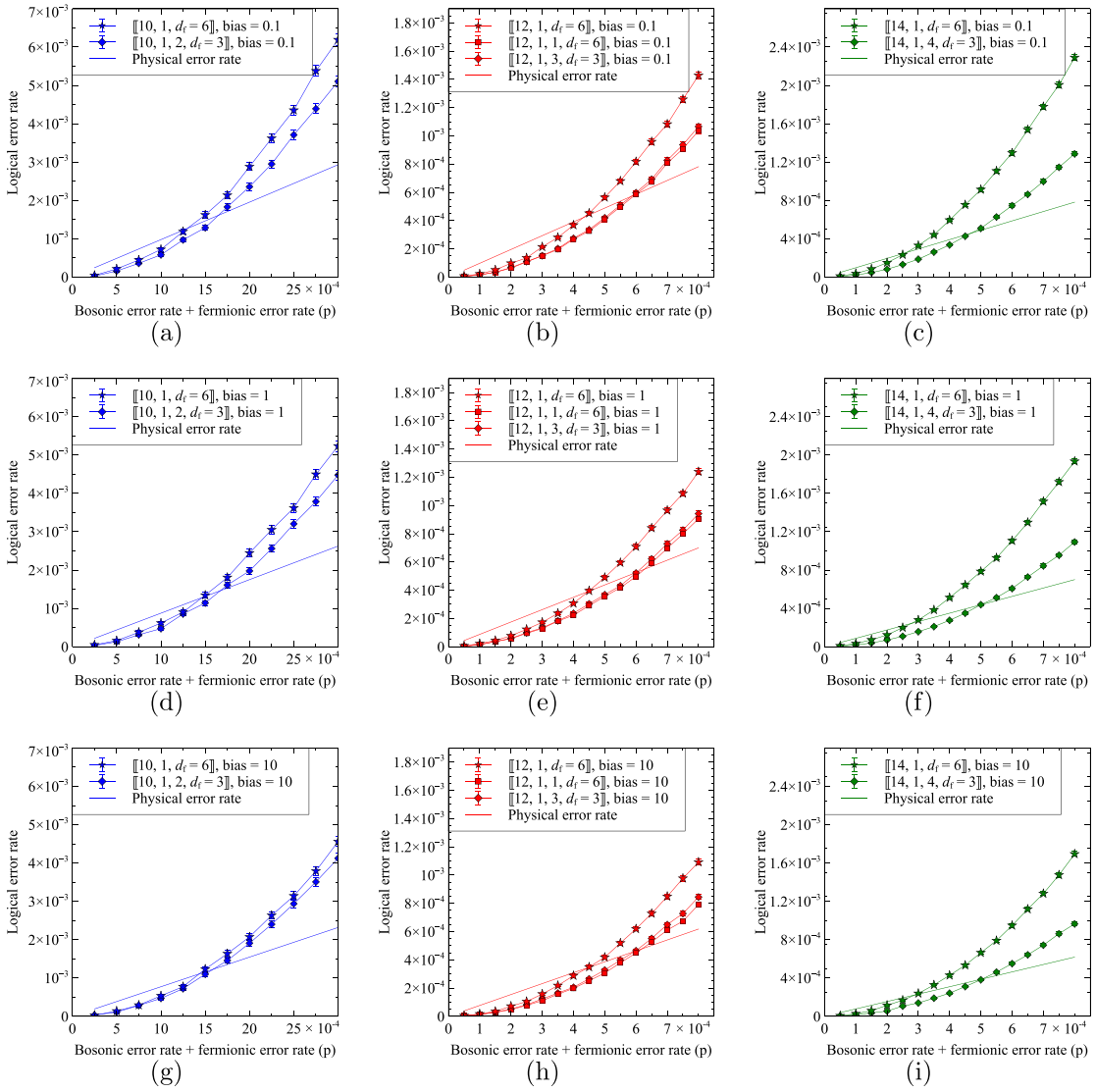

Figure B2. Fault-tolerance logical error plots for currently proposed fermionic subsystem codes as well as previously proposed non-subsystem fermionic codes. The left column shows the plot for the five tetron codes, the middle column shows the plot for the six tetron codes, and the right column shows the plot for the seven tetron codes. The graphs also show the 95% confidence intervals. (Top row) The three plots show the variation of logical error rate with p for bias $\eta = 0.1$. (Middle row) The three plots show the variation of logical error rate with p for bias $\eta = 1$. (Bottom row) The three plots show the variation of logical error rate with p for bias $\eta = 10$.

ORCID iD

Sourav Kundu https://orcid.org/0000-0002-2912-0159

References

[1] Kitaev A 2001 Unpaired Majorana fermions in quantum wires *Phys.-Usp.* **44** 131
[2] Kitaev A 2003 Fault-tolerant quantum computation by anyons *Ann. Phys., NY* **303** 2–30
[3] Kitaev A 2006 Anyons in an exactly solved model and beyond *Ann. Phys., NY* **321** 2–111
[4] Nayak C, Simon S H, Stern A, Freedman M and Das Sarma S 2008 Non-Abelian anyons and topological quantum computation *Rev. Mod. Phys.* **80** 1083
[5] Sau J D, Lutchyn R M, Tewari S and Das Sarma S 2010 Generic new platform for topological quantum computation using semiconductor heterostructures *Phys. Rev. Lett.* **104** 040502
[6] Bravyi S, Terhal B M and Leemhuis B 2010 Majorana fermion codes *New J. Phys.* **12** 083039
[7] Alicea J 2012 New directions in the pursuit of Majorana fermions in solid state systems *Rep. Prog. Phys.* **75** 076501
[8] Leijnse M and Flensberg K 2012 Introduction to topological superconductivity and Majorana fermions *Semicond. Sci. Technol.* **27** 124003
[9] Mong R S K *et al* 2014 Universal topological quantum computation from a superconductor-Abelian quantum Hall heterostructure *Phys. Rev.* X **4** 011036

[10] Das Sarma S, Freedman M and Nayak C 2015 Majorana zero modes and topological quantum computation *npj Quantum Inf.* **1** 1–13
[11] Aasen D *et al* 2016 Milestones toward Majorana-based quantum computing *Phys. Rev.* X **6** 031016
[12] Lutchyn R M, Bakkers E P, Kouwenhoven L P, Krogstrup P, Marcus C M and Oreg Y 2018 Majorana zero modes in superconductor-semiconductor heterostructures *Nat. Rev. Mater.* **3** 52–68
[13] Flensberg K, von Oppen F and Stern A 2021 Engineered platforms for topological superconductivity and Majorana zero modes *Nat. Rev. Mater.* **6** 944–58
[14] Aghaee M *et al* (Microsoft Quantum) 2023 InAs-Al hybrid devices passing the topological gap protocol *Phys. Rev.* B **107** 245423
[15] Karzig T *et al* 2017 Scalable designs for quasiparticle-poisoning-protected topological quantum computation with Majorana zero modes *Phys. Rev.* B **95** 235305
[16] Litinski D and von Oppen F 2017 Braiding by Majorana tracking and long-range CNOT gates with color codes *Phys. Rev.* B **96** 205413
[17] Litinski D and von Oppen F 2018 Quantum computing with Majorana fermion codes *Phys. Rev.* B **97** 205404
[18] Knapp C, Beverland M, Pikulin D I and Karzig T 2018 Modeling noise and error correction for Majorana-based quantum computing *Quantum* **2** 88
[19] Karzig T, Oreg Y, Refael G and Freedman M H 2019 Robust Majorana magic gates via measurements *Phys. Rev.* B **99** 144521
[20] Viyuela O, Vijay S and Fu L 2019 Scalable fermionic error correction in Majorana surface codes *Phys. Rev.* B **99** 205114
[21] Kundu S and Reichardt B W 2023 Majorana qubit codes that also correct odd-weight errors (arXiv:2311.01779)
[22] Hastings M B 2017 Small Majorana fermion codes *Quantum Inf. Comput.* **17** 1191–205
[23] Vijay S and Fu L 2017 Quantum error correction for complex and Majorana fermion qubits (arXiv:1703.00459)
[24] Bomantara R W and Gong J 2020 Combating quasiparticle poisoning with multiple Majorana fermions in a periodically-driven quantum wire *J. Phys.: Condens. Matter* **32** 435301
[25] Roffe J, White D R, Burton S and Campbell E 2020 Decoding across the quantum low-density parity-check code landscape *Phys. Rev. Res.* **2** 043423
[26] Roffe J 2022 LDPC: Python tools for low density parity check codes (available at: https://pypi.org/project/ldpc/)